

Contents lists available at [ScienceDirect](https://www.sciencedirect.com)

Remote Sensing of Environment

journal homepage: www.elsevier.com/locate/rse

Evaluating global and regional land warming trends in the past decades with both MODIS and ERA5-Land land surface temperature data

You-Ren Wang^{a,*}, Dag O. Hessen^a, Bjørn H. Samset^b, Frode Stordal^a

^a Centre for Biogeochemistry in the Anthropocene, University of Oslo, Oslo, Norway

^b CICERO Center for International Climate Research, Oslo, Norway

ARTICLE INFO

Edited by Jing M. Chen

Keywords:

MODIS
ERA5-Land
Land surface temperature
Temperature rate of change
Arctic amplification
Permafrost warming
Global warming

ABSTRACT

Global surface temperature has been setting new record highs in the recent decades, imposing increasing environmental challenges for societies and ecosystems worldwide. Global warming rates of the 20th century have been documented by a number of studies, nevertheless, the warming rates in the most recent decades in the 21st century are of particular interest for understanding the ongoing climate change. Analyzing temperature trends demands data with high spatial resolution and broad geographical coverage to allow for analyzing trends and changes on a regional scale. Land Surface Temperature data from NASA MODIS with global resolution of 0.05° and Skin Temperature data from European Centre for Medium-Range Weather Forecasts (ECMWF) ERA5-Land reanalysis with global resolution of 0.1° fulfill these demands. In this study, we analyze the remote-sensing-based MODIS data to estimate land surface temperature change rates over the period 2001–2020 in global, continental, and pixel-wise scales with statistical significance indicated. The model-based ERA5-Land data are also analyzed in parallel, extending the period of analysis back to 1981. These two independently-sourced datasets, one from satellites above the atmosphere and one from combining surface modeling and observations, are shown to produce highly consistent results. It is revealed that the trends in the shorter period 2001–2020 are spatially conforming to the trends in the longer period 1981–2020 despite the shorter time length. For the period 2001–2020, we show that the global average land surface temperature rate of change was 0.26 °C–0.34 °C per decade, with substantially different warming rates in different regions. The Arctic, Europe, and Russia show statistically significant warming in both datasets. The Arctic, in particular, warmed at a rate 2.5–2.8 times the global average, and data in the 40-year period 1981–2020 suggest that warming is accelerating in almost all the continents or large regions. Most noticeably, the two independent datasets both indicate that Arctic permafrost regions had the world's highest warming rate at the onset of the 21st century, reaching >2 °C per decade in some areas.

1. Introduction

The global mean surface temperature (GMST) has increased by 1.1 °C between the 2001–2021 and 1850–1900 periods, with a rate that has accelerated after the 1970s (IPCC, 2021). Specifically, earlier studies have shown that GMST rose by 0.37° and 0.32 °C in the periods 1925–1944 (0.19° per decade) and 1978–1997 (0.16° per decade), respectively (Jones et al., 1999), and global warming occurred at a rate of 0.15 °C–0.20 °C per decade since the late 1970s (Allen et al., 2018; Hansen et al., 2010; Morice et al., 2020). Predictions from climate models, furthermore, forecast that in 2020–2050, the global mean surface temperature can warm up as much as 0.25 °C per decade (Samset

et al., 2020; Tebaldi et al., 2021), and that the Arctic is transitioning away from a cryosphere-dominated system (Landrum and Holland, 2020).

However, not all regions are warming equally. The Arctic has been found to have warmed twice as fast as the global average in recent decades (Cohen et al., 2014; Gulev et al., 2021), and the IPCC AR6 recently concluded that most land areas in the extratropical northern hemisphere have warmed faster than the GMST average over both the 1900–2020 and 1980–2020 periods (Gulev et al., 2021). At more regional scales, particularly in data sparse regions, they also found that considerable uncertainty is introduced by sometimes large differences in trends between different land surface air temperature datasets.

* Corresponding author.

E-mail address: y.r.wang@ibv.uio.no (Y.-R. Wang).

<https://doi.org/10.1016/j.rse.2022.113181>

Received 12 October 2021; Received in revised form 12 June 2022; Accepted 16 July 2022

Available online 28 July 2022

0034-4257/© 2022 The Author(s). Published by Elsevier Inc. This is an open access article under the CC BY license (<http://creativecommons.org/licenses/by/4.0/>).

Building on these known and predicted features of global climate change, this study assesses the day-night-averaged warming status and evolution in the first two decades of the 21st century with 0.1 and 0.05-degree spatial resolution and global land surface coverage, with particular focus on high latitude regions. The use of high spatial resolution data makes it possible to probe into geographical patterns of local warming, which is critical to climate hazards assessments. We used two independent datasets of land surface temperature, allowing us to check the robustness of the data.

The monthly Land Surface Temperature (LST) remote sensing data (Wan et al., 2015) from Moderate Resolution Imaging Spectroradiometer (MODIS, 2022) of NASA have a spatial resolution of $0.05^\circ \times 0.05^\circ$ ($5600 \text{ m} \times 5600 \text{ m}$ at the equator) and global coverage, and have been recognized and well used for land surface temperature estimates for various land regions globally (Benali et al., 2012; Chen et al., 2017; Eleftheriou et al., 2018; Meyer et al., 2016; Zhang et al., 2016). The data were validated by the radiance-based approach to have a mean bias within 1 K in most cases, including lake, vegetation and soil sites in clear-sky conditions (Wan, 2008; Wan and Li, 2008), and were also found to well agree with ground LSTs, with differences comparable, or smaller, than the uncertainties of the ground measurements (Coll et al., 2005).

In addition to MODIS LST data, the monthly Skin Temperature (SKT) reanalysis data (Muñoz Sabater, 2019) from ERA5-Land of ECMWF (ECMWF, 2022), having a resolution of $0.1^\circ \times 0.1^\circ$ and global coverage, were also analyzed in parallel with MODIS LST data to allow analysis of a longer time period. ERA5-Land is a replay of the land component of the ERA5 climate reanalysis, forced by meteorological fields from ERA5. The data are produced under a single simulation, without coupling to the atmospheric module of the ECMWF's Integrated Forecasting System (IFS) or to the ocean wave model of the IFS, and also without data assimilation. ERA5-Land SKT data have been found to have a spatial and temporal averaged difference of 1 K compared to MODIS LST data in the period 2003–2018 (Muñoz-Sabater et al., 2021). ERA5-Land datasets have also been widely used for a variety of land condition assessments (Chen et al., 2021; Crowhurst et al., 2021; Pelosi et al., 2020; Sheridan et al., 2020; Stefanidis et al., 2021). Both MODIS and ERA5-Land datasets are publicly available.

Land surface temperature trends were estimated globally, continentally, and pixel-wise with global average for the time period 2001–2020 using both of the datasets. Rate of temperature change, in $^\circ\text{C}$ per decade, was obtained as the slope of the linear regression through the 20-yr annual mean data in the respective spatial scales. While a 20-yr period can still be affected by internal climate variability, in particular on local and regional scales, the regression allows an evaluation of the significance of emergent trends relative to internal, interannual variability. Based on this, we emphasized the selection of regions with statistically significant temperature rate of change to ensure proper interpretation of trends.

The common period of MODIS vs. ERA5-Land is the 20 years from 2001 to 2020. In order to explore warming trends over a longer period, we also analyzed the full 40-yr data available in the ERA5-Land database from 1981 to 2020. The difference between the warming trends of the full 40 years and the most recent 20 years was also examined.

2. Data and methodology

2.1. MODIS LST dataset

We used MODIS product MOD11C3 v006 level-3 data distributed by NASA's Land Processes Distributed Active Archive Center (LP DAAC) (MODIS) for the MODIS version of land surface temperature. The MOD11C3 Version 6 product provides monthly Land Surface Temperature and Emissivity (LST&E) values in a 0.05° (5600 m at the equator) latitude/longitude Climate Modeling Grid (CMG), available from February 2000 onwards. The LST&E values in the MOD11C3 product are

derived by compositing and averaging the values from the corresponding month of MOD11C1 daily files. In this product, cloud-contaminated LST values were removed (cloud-masked) to include only clear-sky conditions in the level-3 data at a confidence $\geq 95\%$ over land $\leq 2000 \text{ m}$, or $\geq 66\%$ over land $>2000 \text{ m}$, and at a confidence of $\geq 66\%$ over lakes (Wan, 2013). Statistical and viewing angle dependence analyses of the retrieved surface emissivity values indicate that the Version 6 level-3 LST products are much better in providing more stable results than the previous Version 4.1 and Version 5 products (Wan, 2014). Monthly Day LST and Night LST were averaged to yield the mean LST of the months, and thus the annual mean LST.

2.2. ERA5-Land SKT dataset

We used ERA5-Land product 'Skin temperature' data distributed by Copernicus Climate Change Service (C3S) Climate Data Store (CDS) (ECMWF) for the ERA5-Land version of land surface temperature (Muñoz-Sabater et al., 2021). The data product provides monthly temperature values in a 0.1° ($11,200 \text{ m}$ at the equator) latitude/longitude Climate Modeling Grid (CMG), available from January 1981 onwards. The skin temperature is the theoretical temperature that is required to satisfy the surface energy balance. It represents the temperature of the uppermost surface layer, which has no heat capacity and so can respond instantaneously to changes in surface fluxes. Monthly SKT data were averaged to yield annual mean SKT.

2.3. Pixel selection criteria

MODIS monthly LST data are available for each of the $0.05^\circ \times 0.05^\circ$ pixels throughout the global land, except for those that were cloud-masked. We required that for the computation of global or regional yearly mean of MODIS LST and ERA5-Land SKT, only pixels that have valid (non-cloud-masked) data in each month are taken into account to avoid bias. A pixel that does not meet the requirement was omitted in both data and area when the global/regional mean of that year is calculated. Pixels that do not meet the criteria are shown in blank in the figures.

2.4. Geographical weighting

The longitudinal length of a fixed-angle rectangle decreases as the pixel goes from the equator toward the poles. Consequently, the area of a pixel also reduces along the path. Therefore, when calculating an average quantity over an area using fixed-angle grids (pixels), the geographical weighting factor, namely the area of a pixel in this study, was applied to account for the area difference of pixels in different latitudes.

2.5. Temperature rate of change and significance

There are various statistical methods that can be used for the study of temperature trends. BFAST (Verbesselt et al., 2010) and Greenbrown (Forkel et al., 2013), for example, are methods that can remove seasonal variations and identify temperature breakpoints or anomalies in the temperature time series (Akinyemi et al., 2019; Muro et al., 2018). Here in this work, since the purpose is to understand the general trends of temperature in the past decades in global land areas, we adopted the simple linear regression for estimating temperature rate of change throughout this study. Given the 20 pairs of LST-year (and SKT-year) data in 2001–2020: (LST_i, Y_i) , $i = 1, \dots, 20$, the relationship between LST_i and Y_i can be modelled as:

$$LST_i = \alpha + \beta Y_i + \varepsilon_i \quad (1)$$

where α , β , and ε are the modelled intercept, slope and error term, respectively.

The slope of regression was defined as the temperature rate of change in the unit of $^{\circ}\text{C}/\text{decade}$ in this study. P -value was used to determine the statistical significance of the linear regression. We set the alpha level of p -value to be 0.05, below which the regressed temperature rate of change being due to random chance is lower than 5%, and is therefore statistically significant. R-squared measures the goodness-of-fit for linear regression models, indicating the percentage of the variance explained by the models. Slope, intercept, p -value and r -squared in the regression were all calculated using the function 'scipy.stats.linregress' in Python language version 3.7.4.

2.6. Classification of land regions on earth

Based on the land regions defined in the RECCAP project (Canadell et al., 2011; Ciais et al., 2021), the terrestrial land masses are classified into nine regions in this study as shown in Fig. 1. For each of the nine terrestrial land regions and for each of the 20 years, annual mean MODIS and ERA5-Land temperatures were calculated as area weighted averages over all the pixels within the respective region, and temperature rate of change for each region was respectively analyzed by regression.

3. Results

3.1. Global temperature distributions in the period 2001–2020

There are intrinsic differences between the two datasets. The datasets utilize different algorithms and parameters in data measurement and modeling techniques. Furthermore, MODIS data are cloud-free, while ERA5-Land data are available in any cloud conditions. These all will result in variability and uncertainty in reporting land surface temperature data. Therefore, before performing regression analysis for temperature rate of change, we examined global temperature distributions in the period 2001–2020 from both of the datasets for the evaluation of consistency.

Fig. 2a displays the global distribution of MODIS LST averaging over 2001–2020. Blank pixels are those that do not have valid data for at least one full year during the period due to persistent cloud blockage to the satellites. Mean LST of the past two decades worldwide ranges from

$-63\text{ }^{\circ}\text{C}$ to $41\text{ }^{\circ}\text{C}$, depending on latitudes and geographical features. Similarly, Fig. 2b displays the global distribution of ERA5-Land SKT averaging over the same period, showing mean SKT values ranging from $-58\text{ }^{\circ}\text{C}$ to $40\text{ }^{\circ}\text{C}$. Despite their independent data sources, the comparison between Fig. 2a and b shows prominent similarity in the spatial patterns of MODIS and ERA5-Land temperature distributions.

The relative and absolute difference between the two datasets are provided in Fig. 2c and d, respectively. Fig. 2c indicates that ERA5-Land tends to estimate temperature lower than MODIS does in barren lands, while in cryosphere regions, ERA5-Land tends to estimate higher. Fig. 2d shows that for most of the lands, the absolute difference between the two temperature estimates is within approximately $2\text{ }^{\circ}\text{C}$ (in blue). The highest absolute difference occurred mostly in Antarctica, Greenland, and the Tibetan Plateau, reaching as high as $6\text{ }^{\circ}\text{C}$ or more.

For the temperature time series 2001–2020, the Root Mean Square Error (RMSE) as well as the correlation coefficient between the two datasets were also studied. Only pixels with a full length of 20-year valid data were examined. The results show that the RMSE distribution (Fig. 2e) is very similar to the distribution of the absolute difference (Fig. 2d). Except for Antarctica, most of the land pixels have an RMSE within approximately $2\text{ }^{\circ}\text{C}$ (in blue). Most of the correlation coefficients (Fig. 2f) of pixels have a value higher than 0.8. Both of the distributions indicate a good consistency between the datasets in the 20-yr time series despite the intrinsic differences in data sources.

3.2. Temperature rate of change in global and regional scales

3.2.1. MODIS and ERA5-Land in the period 2001–2020

The change rates of MODIS and ERA5-Land temperatures in 2001–2020 were estimated globally and regionally using the yearly mean temperatures in the period. Global and regional temperature rate of change obtained as the slope of the regression as well as the p -values and r^2 are summarized in Table 1 for both MODIS and ERA5-Land temperatures.

MODIS and ERA5-Land yearly mean temperatures are shown side by side for each region. As a result, both of the datasets reveal that only the Arctic, Russia, Europe, and the Global mean temperature have temperature change rates that are statistically significant among all continents

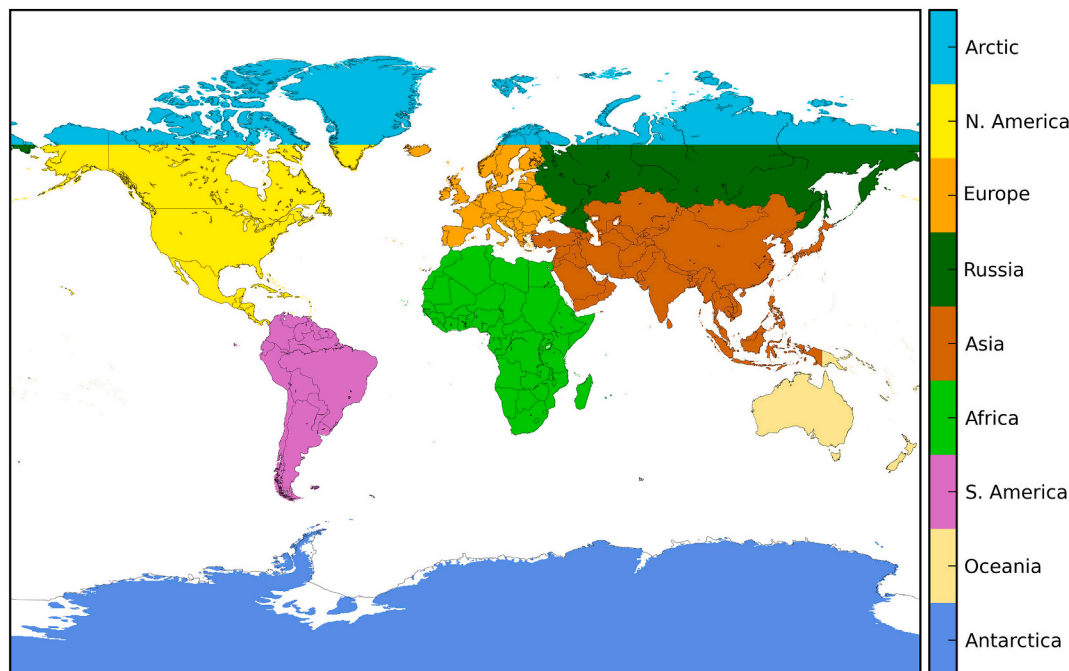


Fig. 1. Classification of nine regions of the world used in this study. North America, Europe, and Russia refer to their regions excluding the parts in the Arctic.

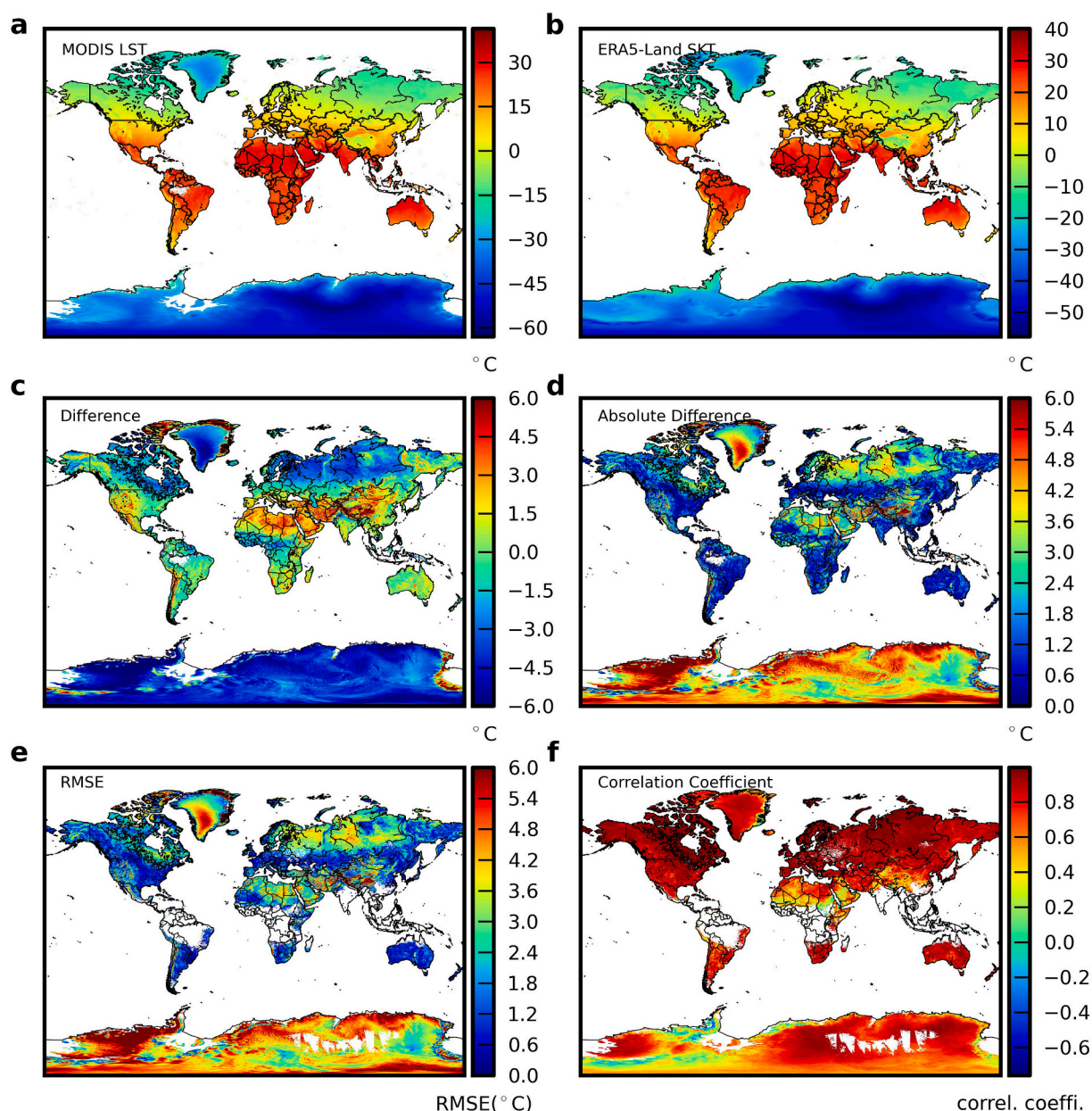


Fig. 2. Global land surface temperatures in 2001–2020. (a) From MODIS LST. (b) From ERA5-Land SKT. (c) Difference between the 20-yr mean MODIS LST and mean ERA5-Land SKT, shown as the former subtracted by the latter. (d) Panel (c) shown in absolute values. (e) RMSE between MODIS and ERA5-Land in the period 2001–2020. (f) Correlation coefficient between MODIS and ERA5-Land in the period 2001–2020. MODIS data were resampled in the grid of ERA5-Land before performing the comparisons in (c), (d), (e) and (f).

and regions in the period 2001–2020. North America and Antarctica are found by both datasets to have insignificant rate of change. Asia, Africa, South America, and Oceania are not significant in MODIS but significant in ERA5-Land. This could reflect that MODIS data in these regions often have areas blocked by clouds in different years, which causes fluctuation in the yearly mean values in those regions and thus increases their p -values. On the contrary, ERA5-Land data do not have the issue of clouds, and therefore the yearly means are more stable and thus more likely to yield significant trends.

With both datasets considered, the global mean land temperature had an average rate of change of 0.26–0.34 °C/decade in 2001–2020. The fastest regional warming occurred in the Arctic with a rate of 0.72–0.86 °C/decade, which are 2.5–2.8 times the global average, while Russia and Europe had temperature change rates up to 2.5 and 2.4 times the global averages, respectively.

3.2.2. ERA5-Land in the period 1981–2020

In order to assess the trends of temperature in a longer time period, the full 40-yr data available in ERA5-Land for the period 1981–2020 were also analyzed (Table 2).

The results indicate that all the regions had significant temperature change rates in the period, with most of their p -values much lower than 0.05. Similar to the period in 2001–2020, regions having the highest rate of change are the Arctic, Europe, and Russia in the 40-yr period. It is noticeable that in these three regions, the rates of temperature change in the 40-yr period 1981–2020 are lower than that in the latter half of the 40-yr period. This is true also for other regions except for Asia and Africa.

The comparison between rate of temperature change over the past 20-yr and the 40-yr period reveals that global and continental warming rates were not constant through the past decades (Fig. S1).

Table 1

Global and regional yearly mean land temperature (°C) and rate of change from MODIS and ERA5-Land datasets for the 20-yr period 2001–2020. Categories with p-value <0.05 in the regression for rate of change are shown in red, indicating statistically significant trends of temperature change.

	Global		Arctic		N. America		Europe		Russia		Asia		Africa		S. America		Oceania		Antarctica	
	MODIS	ERA5	MODIS	ERA5	MODIS	ERA5	MODIS	ERA5	MODIS	ERA5	MODIS	ERA5	MODIS	ERA5	MODIS	ERA5	MODIS	ERA5	MODIS	ERA5
2001	7.2	9.2	-16.4	-14.8	6.3	6.9	7.9	8.5	-4.5	-2.8	14.9	15.1	27.0	25.5	20.3	21.9	23.3	23.1	-40.8	-37.0
2002	8.0	9.4	-16.1	-14.8	5.7	6.4	8.7	9.0	-3.9	-2.3	15.7	15.3	26.6	25.7	20.6	22.2	24.3	24.3	-40.0	-36.2
2003	7.7	9.3	-15.6	-14.2	6.2	6.7	8.6	8.7	-3.7	-2.0	14.8	14.9	26.7	25.8	20.4	22.2	24.1	24.0	-40.9	-37.1
2004	7.4	9.2	-17.0	-15.4	5.7	6.2	8.0	8.6	-4.3	-2.5	15.4	15.3	26.5	25.6	19.9	22.1	23.7	23.8	-41.2	-37.3
2005	7.8	9.6	-15.2	-13.6	6.2	7.0	8.2	8.5	-3.4	-1.8	14.8	15.1	26.7	26.0	20.1	22.2	24.5	24.6	-40.6	-36.7
2006	7.6	9.4	-15.7	-14.2	6.8	7.4	8.4	8.9	-4.9	-2.9	15.4	15.5	26.5	25.5	20.2	22.2	23.7	23.8	-41.2	-37.2
2007	7.9	9.6	-15.4	-13.9	5.8	6.6	9.1	9.3	-2.9	-1.1	15.6	15.5	26.6	25.6	20.2	22.1	24.1	23.9	-40.2	-36.5
2008	7.5	9.3	-15.9	-14.3	5.3	6.1	8.7	9.1	-3.2	-1.4	15.0	15.2	26.6	25.5	20.1	22.1	23.6	23.8	-40.7	-37.5
2009	7.7	9.4	-16.0	-14.8	5.7	6.2	8.3	9.0	-4.5	-2.8	15.4	15.4	26.8	25.9	20.5	22.3	24.0	24.2	-40.3	-36.5
2010	7.7	9.5	-14.6	-13.3	6.4	7.3	7.3	7.9	-4.5	-2.9	15.1	15.5	27.1	26.3	20.6	22.4	23.2	23.2	-41.5	-37.5
2011	7.3	9.3	-15.3	-13.7	5.9	6.7	8.9	9.1	-3.5	-1.9	14.4	14.9	26.6	25.6	19.7	22.0	22.5	22.8	-40.1	-36.5
2012	7.4	9.4	-14.9	-13.5	6.9	7.4	8.4	8.8	-4.0	-2.2	14.2	14.8	26.6	25.7	20.4	22.3	23.6	23.6	-41.1	-37.4
2013	7.8	9.5	-15.7	-14.5	5.7	6.4	8.5	8.8	-3.6	-1.8	15.0	15.2	27.0	25.9	20.9	22.2	25.0	24.7	-40.5	-36.6
2014	7.7	9.4	-15.5	-14.2	5.7	6.4	9.4	9.7	-3.7	-2.1	15.3	15.2	27.1	25.9	20.8	22.3	24.5	24.3	-40.9	-37.2
2015	8.1	9.7	-15.7	-14.2	6.4	7.0	9.5	9.7	-2.9	-1.2	16.0	15.5	27.0	26.1	21.2	22.7	24.3	24.3	-41.7	-37.5
2016	8.1	10.0	-14.0	-12.6	6.9	7.6	8.8	9.3	-3.4	-1.6	15.3	15.7	27.1	26.4	20.7	22.6	24.2	24.1	-41.0	-36.8
2017	7.8	9.8	-15.1	-13.3	6.4	7.3	8.9	9.3	-3.2	-1.4	15.5	15.6	26.6	26.1	20.3	22.5	24.1	24.3	-41.4	-37.0
2018	7.6	9.7	-15.5	-13.7	5.9	6.7	9.3	9.7	-3.6	-2.0	15.0	15.5	26.5	26.1	20.1	22.3	24.4	24.6	-40.7	-36.3
2019	8.2	9.9	-14.6	-13.0	5.9	6.7	9.4	9.9	-3.1	-1.2	15.7	15.6	26.7	26.2	20.7	22.7	24.9	25.3	-40.8	-36.5
2020	8.3	10.1	-14.6	-12.6	6.3	7.1	9.7	10.2	-2.0	-0.2	15.6	15.5	26.6	26.1	20.8	22.8	24.3	24.4	-40.7	-36.1
mean	7.7	9.5	-15.4	-13.9	6.1	6.8	8.7	9.1	-3.6	-1.9	15.2	15.3	26.7	25.9	20.4	22.3	24.0	24.1	-40.8	-36.9
p-value	0.011	0.000	0.002	0.000	0.446	0.234	0.002	0.000	0.007	0.006	0.342	0.034	0.591	0.001	0.065	0.000	0.116	0.040	0.254	0.359
R-squared	0.31	0.64	0.41	0.50	0.03	0.08	0.42	0.52	0.34	0.35	0.05	0.23	0.02	0.47	0.18	0.61	0.13	0.21	0.07	0.05
°C/decade	0.26	0.34	0.72	0.86	0.13	0.20	0.62	0.63	0.65	0.68	0.16	0.20	0.05	0.31	0.25	0.32	0.34	0.43	-0.20	0.16

Table 2

Global and regional yearly mean land temperature (°C) and rate of change from ERA5-Land dataset for the 40-yr period 1981–2020. Categories with p -value < 0.05 in the regression for rate of change are shown in red.

	Global	Arctic	N. America	Europe	Russia	Asia	Africa	S. America	Oceania	Antarctica
	EAR5-Land	EAR5-Land	EAR5-Land	EAR5-Land	EAR5-Land	EAR5-Land	EAR5-Land	EAR5-Land	EAR5-Land	EAR5-Land
1981	9.0	-14.6	7.0	7.8	-2.3	14.6	25.0	21.7	23.5	-36.4
1982	8.5	-16.2	5.2	8.3	-3.0	14.4	24.9	21.7	23.5	-37.4
1983	8.9	-15.5	5.8	8.5	-2.0	14.5	25.3	22.0	23.6	-37.4
1984	8.5	-15.5	5.8	7.9	-3.4	14.1	25.1	21.4	22.9	-36.9
1985	8.5	-15.3	5.5	7.1	-3.7	14.4	24.9	21.5	23.6	-37.7
1986	8.7	-15.8	6.2	7.8	-2.9	14.4	25.0	21.6	23.7	-37.2
1987	8.9	-15.9	6.9	7.2	-4.3	14.8	25.7	22.1	23.6	-37.7
1988	9.1	-14.8	6.3	8.3	-2.2	14.9	25.3	21.9	24.0	-36.9
1989	8.8	-15.6	5.8	9.2	-1.9	14.6	25.0	21.7	23.3	-37.4
1990	9.2	-15.5	6.2	9.2	-2.0	15.0	25.6	21.9	23.9	-36.9
1991	9.1	-15.1	6.4	8.2	-2.3	14.8	25.3	21.8	24.0	-36.4
1992	8.6	-16.2	5.8	8.6	-2.7	14.2	25.1	21.6	23.2	-37.1
1993	8.7	-15.2	5.9	7.9	-2.9	14.3	25.3	21.8	23.4	-37.8
1994	8.9	-15.4	6.3	8.9	-3.1	14.8	25.2	22.0	23.7	-37.8
1995	9.2	-14.4	6.4	8.5	-1.3	14.9	25.5	22.1	23.2	-37.5
1996	8.8	-14.8	5.7	7.5	-3.2	14.4	25.3	21.8	23.7	-36.6
1997	8.9	-15.1	6.1	8.3	-2.7	14.7	25.3	22.1	23.5	-37.7
1998	9.3	-15.2	7.3	8.3	-3.4	15.3	25.8	22.5	24.0	-37.6
1999	9.0	-15.6	6.9	8.8	-3.0	15.2	25.4	21.7	23.2	-37.6
2000	8.9	-15.1	6.5	9.2	-2.9	14.8	25.2	21.5	22.6	-37.4
2001	9.2	-14.8	6.9	8.5	-2.8	15.1	25.5	21.9	23.1	-37.0
2002	9.4	-14.8	6.4	9.0	-2.3	15.3	25.7	22.2	24.3	-36.2
2003	9.3	-14.2	6.7	8.7	-2.0	14.9	25.8	22.2	24.0	-37.1
2004	9.2	-15.4	6.2	8.6	-2.5	15.3	25.6	22.1	23.8	-37.3

To look more closely into the temperature change rates obtained from different periods, we further analyzed the earlier 20-yr period 1981–2000 for comparison (Table 3).

Unlike in the latest 20-yr period 2001–2020, in the earlier 20-yr period 1981–2000, only Asia and Africa had significant temperature change rates.

Comparing the results of warming rates of the three different periods, it is summarized that the later 20-yr period 2001–2020 had stronger and more significant warming trends than the earlier 20-yr period 1981–2000 in most of the regions in the world. This suggests that global and regional warming is accelerating in the past decades.

3.3. Temperature rate of change in the Arctic by month

3.3.1. MODIS and ERA5-Land in the period 2001–2020

The enhanced and accelerated warming in the Arctic, in comparison with that for the entire globe, is known as Arctic amplification (Serreze and Francis, 2006). It is commonly attributed to sea-ice loss (Parmentier et al., 2013), fast atmospheric processes (Previdi et al., 2020), and ocean heat transport (van der Linden et al., 2019). To study the seasonal dependence of terrestrial Arctic amplification, we averaged temperatures of all the land pixels located above 66.5°N and analyzed the temperature change rate in the 20 years for each month.

Fig. 3a and b show the monthly mean temperature for March to August in 2001–2020, respectively from MODIS and from ERA5-Land temperatures, while Fig. 3c and d are for September to February.

Fig. 3e indicates that the trends of monthly temperature rate of change along the year are consistent in the two datasets. February and April appear to be the two months that had the fastest warming trends in both of the datasets, with rates between 1.16 and 1.67 °C/decade. The terrestrial Arctic warmed up the fastest in late winter to early spring, and the slowest in the summer in the past two decades. December and July were the two months that had the lowest rate of change. Global mean temperature rate of change by month are also shown, revealing the pronounced Arctic amplification.

3.3.2. Statistical significance of temperature trends obtained from different time scales

The 40-yr temperature data available in ERA5-Land provide the opportunity to examine temperature rate of change in the Arctic in different time scales. As shorter time periods may not be sufficient to yield statistically significant temperature rates of change, we checked the p -values of the regressions of various time scales to probe the relation between the length of time period and the level of significance.

The whole period of 1981–2020 can be divided into four 10-yr periods, three 20-yr periods, two 30-yr periods, or one 40-yr period. Temperature rate of change for each month in each period has an associated p -value when performing regression analysis (Table S1).

It is noticeable that longer periods tend to cause more months to have a statistically significant rate of change. The frequency of the appearance of p -values lower than 0.05 reveals that the two 30-yr periods and the 40-year period yield a statistically significant temperature rate of

Table 3

Global and regional yearly mean land temperature (°C) and rate of change from ERA5-Land dataset for the earlier 20-yr period 1981–2000. Categories with *p*-value <0.05 in the regression for rate of change are shown in red.

	Global	Arctic	N. America	Europe	Russia	Asia	Africa	S. America	Oceania	Antarctica
	EAR5-Land	EAR5-Land	EAR5-Land	EAR5-Land	EAR5-Land	EAR5-Land	EAR5-Land	EAR5-Land	EAR5-Land	EAR5-Land
1981	9.0	-14.6	7.0	7.8	-2.3	14.6	25.0	21.7	23.5	-36.4
1982	8.5	-16.2	5.2	8.3	-3.0	14.4	24.9	21.7	23.5	-37.4
1983	8.9	-15.5	5.8	8.5	-2.0	14.5	25.3	22.0	23.6	-37.4
1984	8.5	-15.5	5.8	7.9	-3.4	14.1	25.1	21.4	22.9	-36.9
1985	8.5	-15.3	5.5	7.1	-3.7	14.4	24.9	21.5	23.6	-37.7
1986	8.7	-15.8	6.2	7.8	-2.9	14.4	25.0	21.6	23.7	-37.2
1987	8.9	-15.9	6.9	7.2	-4.3	14.8	25.7	22.1	23.6	-37.7
1988	9.1	-14.8	6.3	8.3	-2.2	14.9	25.3	21.9	24.0	-36.9
1989	8.8	-15.6	5.8	9.2	-1.9	14.6	25.0	21.7	23.3	-37.4
1990	9.2	-15.5	6.2	9.2	-2.0	15.0	25.6	21.9	23.9	-36.9
1991	9.1	-15.1	6.4	8.2	-2.3	14.8	25.3	21.8	24.0	-36.4
1992	8.6	-16.2	5.8	8.6	-2.7	14.2	25.1	21.6	23.2	-37.1
1993	8.7	-15.2	5.9	7.9	-2.9	14.3	25.3	21.8	23.4	-37.8
1994	8.9	-15.4	6.3	8.9	-3.1	14.8	25.2	22.0	23.7	-37.8
1995	9.2	-14.4	6.4	8.5	-1.3	14.9	25.5	22.1	23.2	-37.5
1996	8.8	-14.8	5.7	7.5	-3.2	14.4	25.3	21.8	23.7	-36.6
1997	8.9	-15.1	6.1	8.3	-2.7	14.7	25.3	22.1	23.5	-37.7
1998	9.3	-15.2	7.3	8.3	-3.4	15.3	25.8	22.5	24.0	-37.6
1999	9.0	-15.6	6.9	8.8	-3.0	15.2	25.4	21.7	23.2	-37.6
2000	8.9	-15.1	6.5	9.2	-2.9	14.8	25.2	21.5	22.6	-37.4
mean	8.9	-15.3	6.2	8.3	-2.8	14.7	25.3	21.8	23.5	-37.3
p-value	0.063	0.266	0.109	0.095	0.967	0.013	0.035	0.123	0.495	0.202
R-squared	0.18	0.07	0.14	0.15	0.00	0.30	0.22	0.13	0.03	0.09
°C/decade	0.16	0.20	0.31	0.38	-0.01	0.28	0.19	0.15	-0.10	-0.22

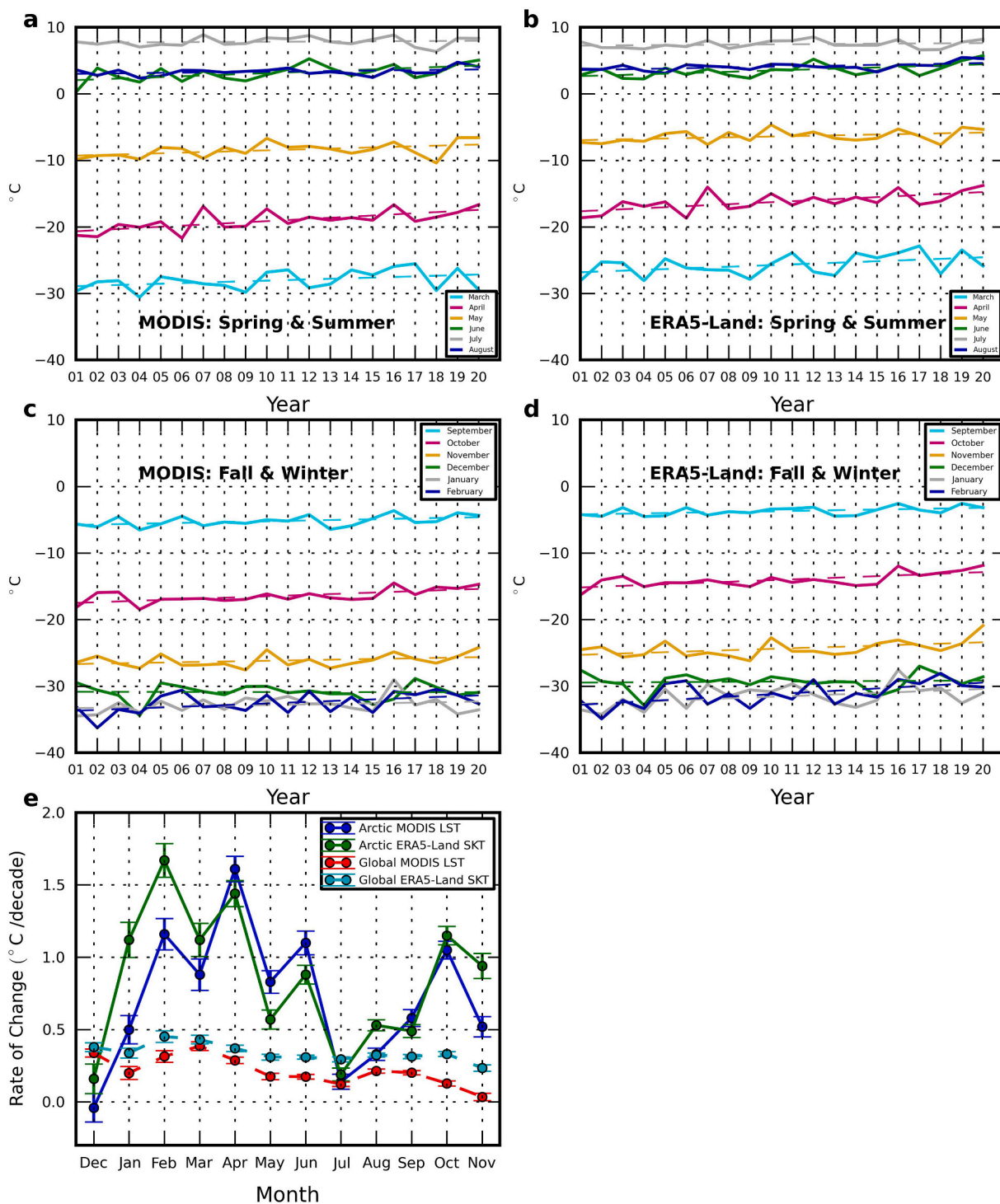


Fig. 3. Monthly land temperature averaged in the Arctic in 2001–2020 from MODIS LST and ERA5-Land SKT and temperature rate of change by month. (a) From MODIS for March to August (b) From ERA5-Land for March to August. (c) From MODIS for September to February. (d) From ERA5-Land for September to February. (e) Arctic temperature rate of change by month from MODIS and ERA-Land temperatures, where error bars indicate ± 2 standard error for 95% confidence interval from the regression for the rate of change of each month. Global mean temperature change rates by month are also shown for comparison.

change for almost all the months. Temperature rate of change by month, therefore, was evaluated by 30-year and 40-year periods in 3.3.3.

3.3.3. Temperature rate of change evaluated by 30-year and 40-year periods

When comparing temperatures in the latest 30-yr period (1991–2020) with that of the earlier 30-yr period (1981–2010) in the

Arctic, it is evident that the later period had higher temperature rates of change in almost all the months. And the full 40-yr curve appears to be the “average” curve of the earlier 30-yr curve and the later 30-yr curve, as expected. (Fig. 4).

This reveals that warming is faster in the later years than in the earlier years. With the full 40-year data available in ERA5-Land, we show that warming is accelerating in the Arctic in almost all the months.

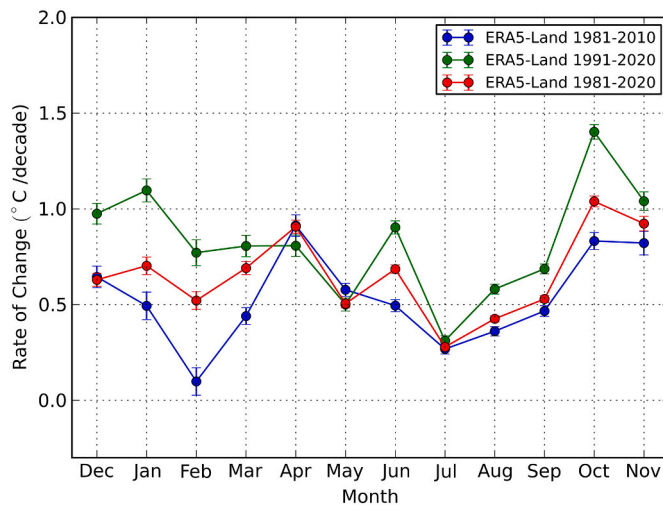


Fig. 4. Temperature trends in the Arctic obtained by two 30-yr periods and one 40-yr period in ERA5-Land. Error bars indicate ± 2 standard error for 95% confidence interval from the regression for the rate of change of each month.

3.4. Temperature rate of change in pixel scale

3.4.1. MODIS and ERA5-Land in the period 2001–2020

While the global and regional land temperature rate of change were estimated using the averaged MODIS and ERA5-Land temperatures of the entire region, the individual grid pixels, however, can have variabilities in the trend of temperature change. For a closer spatial analysis, the spatial distributions of temperature trends were studied by checking each pixel worldwide. Similar to the regional assessment, temperature rate of change of a pixel was estimated using linear regression of the 20-yr annual mean data of that pixel, as shown in Fig. 5a and b.

The two distributions share noticeable similarity between MODIS and ERA5-Land. Both of them exhibit distinctive temperature change rates in northern Siberia, northern Alaska, and most of Europe in similar patterns. However, a noticeable divergence was found in Antarctica, where MODIS shows more moderate temperature change rates in cooling and warming, while ERA5-Land shows more considerable warming in large areas.

The p -value of each pixel from the temperature regression for 2001–2020 was also calculated. Fig. 6 displays the global distribution of p -value from MODIS and from ERA5-Land. Pixels with $p < 0.05$ are shown in Fig. 6c and d respectively for MODIS and ERA5-Land temperatures, indicating the locations where the temperature rates of change are statistically significant. Both of the similar distributions reveal that northern Siberia, northern Alaska, Eastern and Central Europe were the regions that had significant and faster rates of warming worldwide over the past two decades. Fig. 5e and f are the Standard Error (SE) of the pixels in the regression for rate of change, respectively for MODIS and ERA5-Land. The two figures show that the SE of most of the pixels is < 0.1 °C for both of the datasets.

3.4.2. ERA5-Land in the period 1981–2020

In order to examine whether the trends obtained in relatively short 20-yr period are representative for extended periods, the full 40-yr data available in ERA5-Land in the period 1981–2020 were analyzed in the same way as for 2001–2020. Temperature rates of change of pixels are indicated in Fig. 7.

Similar to the 20-yr period 2001–2020, pixels in northern Siberia also have the highest rate of change in the 40-yr period 1981–2020. However, unlike the period 2001–2020, pixels in this longer period have significant temperature change rates in 1981–2020 across most of the world.

It is demonstrated that the regional trends obtained from the 40-yr period conform to the results from the 20-yr period of both of the datasets. When the length of the period doubles, more regions were found to display significant warming trends, which are not revealed in the shorter period due to the limitation of data length.

3.4.3. Antarctica in the period 2001–2020

In addition, the polar views of Antarctica showing pixels with statistically significant temperature rate of change are shown in Fig. 8. The distributions from MODIS and from ERA5-Land temperatures in Antarctica are not as consistent as in other regions. However, for a part of the coastal areas (shown by arrows), in the areas where warming permafrost sites have been documented (Biskaborn et al., 2019), both datasets show statistically significant warming trends. The results indicate that warming in Antarctica is mostly confined to a narrow coastal zone, suggesting a critical role of ocean influence (Hellmer et al., 2012; Shepherd et al., 2004) on the thawing of Antarctic permafrost, while inland Antarctica is less affected due to altitudinal effects.

On the other hand, regions with decreasing temperature trends were also revealed. As shown already in Fig. 2(e) and 2(f), MODIS and ERA5-Land differ in large parts of Antarctica.

3.4.4. Circumpolar Arctic region in the period 2001–2020

Further analysis was performed for the fast-warming circumpolar region, where permafrost is located. Fig. 9a and b are the polar views of Fig. 5c and d, exhibiting pronounced conformity between the two datasets in areas having statistically significant temperature trends as well as in the rate of warming of these areas.

Fig. 9c and d are respectively the distributions of permafrost areas (Rekacewicz, 2005) and land cover types (Ahlenius, 2005) in the circumpolar region created by UNEP/GRID-Arendal. By comparison, it is noticeable that the fast warming areas shown in northern Siberia and northern Alaska coincide with the areas of continuous permafrost, indicating that the continuous permafrost has experienced the fastest land surface warming in the world in 2001–2020. This pixel-wise analysis, together with the use of p -value selection to mask the insignificant areas, has generalized the studies of permafrost temperature change rates from scattered borehole locations (Biskaborn et al., 2019) to extended geographical coverage. Fig. 9d further shows that tundra is the dominant land cover in these fast-warming areas.

4. Discussion

4.1. Difference of temperature estimates between MODIS and ERA5-Land

The difference of temperature estimates between the two datasets has previously been studied by difference approaches. The Root Mean Squared Error (RMSE) of temperature estimates between MODIS and ERA5-Land found in (Muñoz-Sabater et al., 2021) has a global pattern similar to the distribution of temperature absolute difference shown in Fig. 2d in this study.

For Antarctica, where the difference is most considerable, Fréville et al., 2014 found a widespread warm difference ranging from +3 to +6 °C in ERA reanalysis data compared to MODIS, and they showed that ERA-Interim/land simulations indicated that the difference may be due primarily to an overestimation of the surface turbulent fluxes in very stable boundary layer conditions.

4.2. Cloud effect

The effect of clouds in affecting temperature rate of change in this work is worth studying. Given the fact that MODIS LST provides data under cloud-free condition only, and ERA5-Land does not have cloud information, we therefore turned to another dataset. The ERA5 SKT dataset, an ECMWF dataset earlier than the ERA5-Land release, has daily data of cloud cover percentage as well as SKT, with a coarser spatial

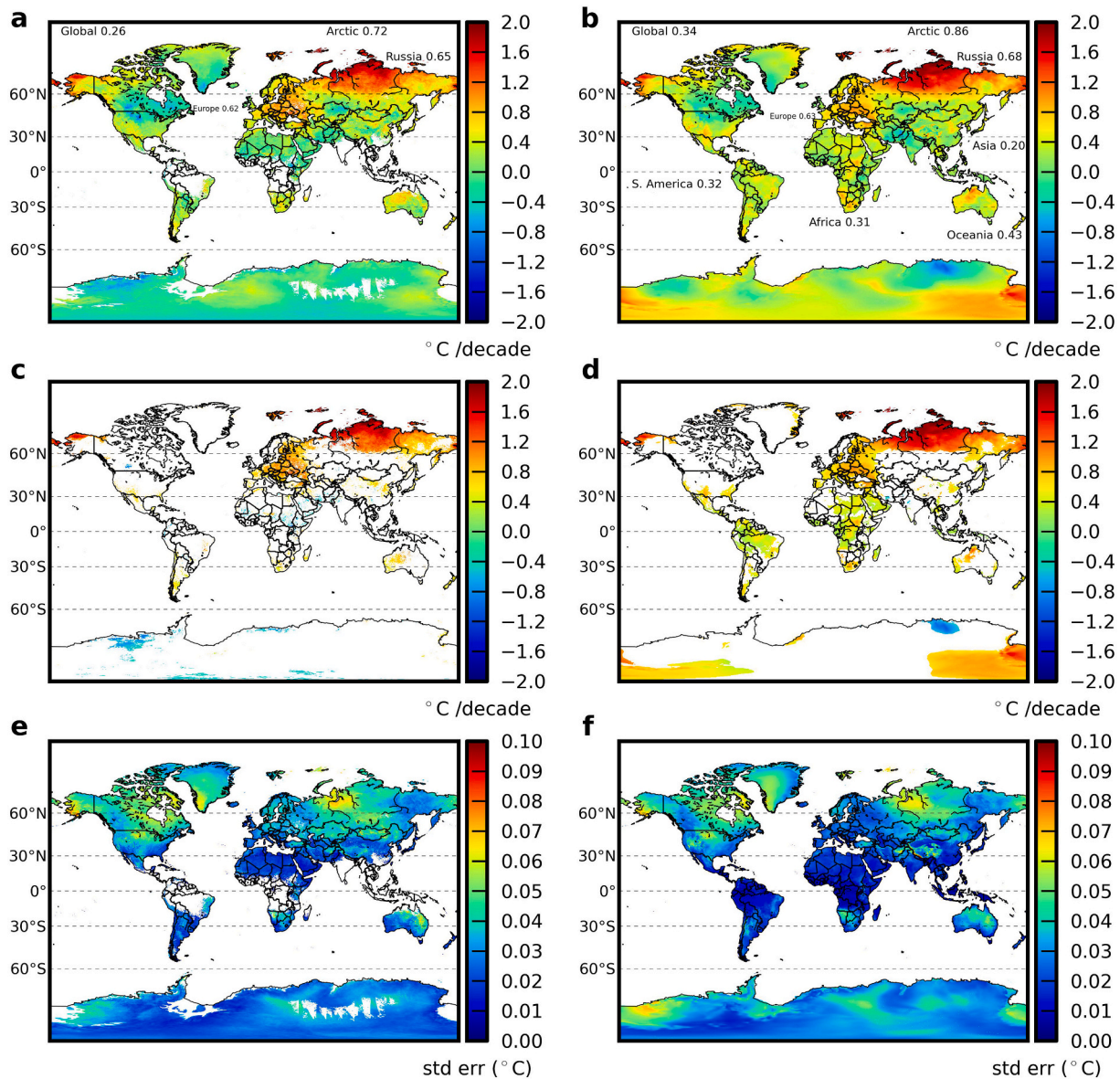


Fig. 5. Land surface temperature rate of change ($^{\circ}\text{C}/\text{decade}$) in 2001–2020 from MODIS LST and ERA5-Land SKT. (a) From MODIS. (b) From ERA5-Land. (c) Pixels with statistically significant trends from MODIS. (d) Pixels with statistically significant trends from ERA5-Land. (e) Standard Error (SE) in the regression for the temperature rate of change of MODIS. (f) SE in the regression for the temperature rate of change of ERA5-Land. Note that in (a) and (e), South America, Africa, South Asia, and northern Australia contain blank areas due to the requirement in this study that a pixel must have 20-yr complete, non-cloud-masked data for performing the regression for temperature rate of change. Regional temperature rates of change that are statistically significant are labeled in (a) and (b).

resolution of $0.25^{\circ} \times 0.25^{\circ}$ than the resolution of ERA5-Land being $0.1^{\circ} \times 0.1^{\circ}$.

To examine the effect of clouds in different levels of cloud cover percentage, we set the thresholds of maximum cloud cover allowance to be 0%, 20%, 50%, and 100%. The cloud cover percentage of a day below the threshold is treated as “cloud-free”, and the monthly SKT of a pixel is determined as the mean of the cloud-free days in the month. Then, global and regional temperature rate of change were obtained from ERA5 SKT dataset with respect to the different level of cloud cover thresholds.

The results suggest that changing the threshold, in general, also changes the temperature rate of change. However, the changes do not cause contradicting results to our main findings using MODIS LST and ERA5-Land SKT. In addition, regardless of the threshold level of cloud cover, the Arctic, Europe, and Russia always have the highest temperature rate of change among all the regions, which is the same as what we obtained in this work. *P*-values also indicate that the rates of change are

highly statistically significant in all the categories, except for a few cloud levels in Antarctica (Fig. S2, Table S2).

4.3. Difference between air temperature and surface temperature

In the research of climate change, air temperature is normally the indicator rather than surface temperature. Our work is based on surface temperature owing to the fact that it is the common temperature product available in both MODIS and ERA5-Land datasets.

In order to assess the difference in global and regional rate of change between air temperature and surface temperature, we used the “ERA5-Land T2M” dataset for temperature 2-m above ground for this purpose.

To obtain global and regional 2-m air temperature rate of change, the dataset was processed in the same procedure performed for ERA5-Land SKT. The results revealed that the trends of T2M and SKT temperatures are very similar in global and regional scales, even with very close *p*-values (Table S3).

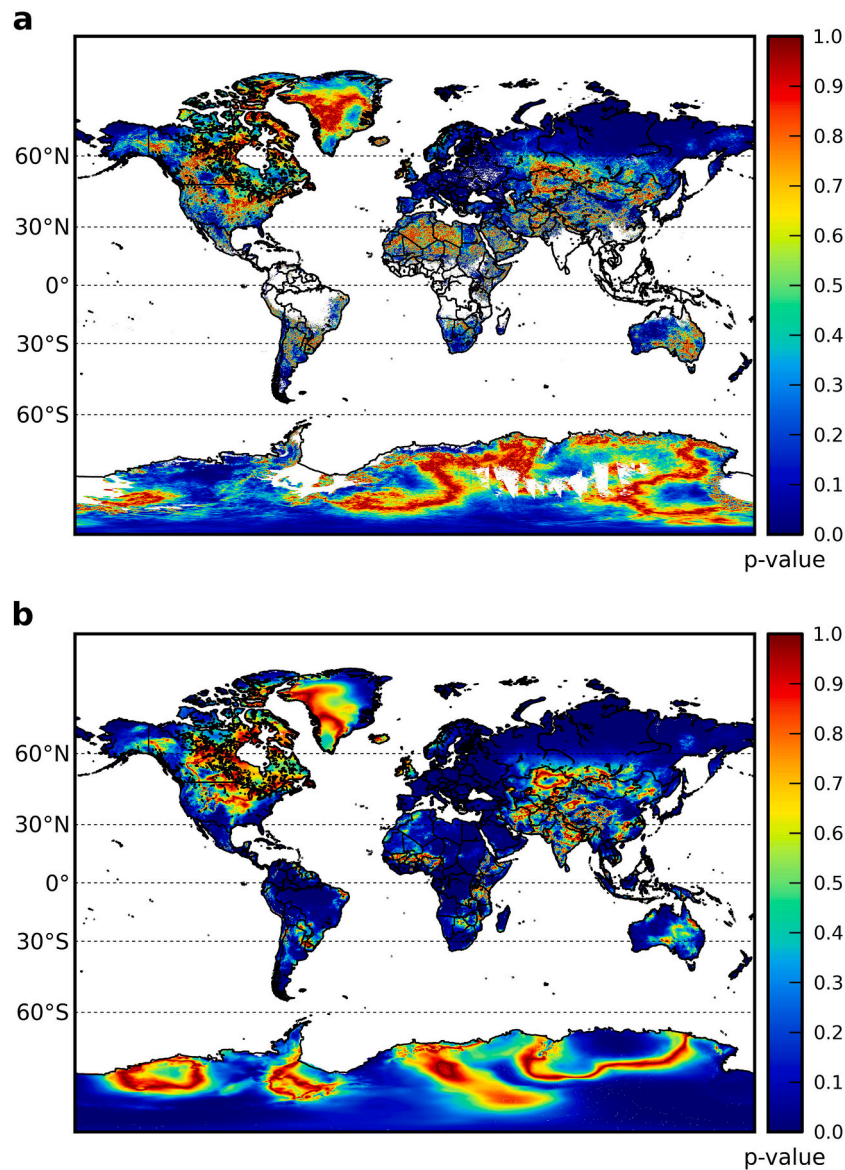


Fig. 6. Global distribution of p -value from temperature regression analysis for 2001–2020. (a) From MODIS LST. Blank areas are pixels that do not have 20-year complete, non-cloud-masked data for performing the regression for temperature rate of change. (b) From ERA5-Land SKT.

Thus, the temperature trends shown in this work using MODIS LST and ERA5-Land SKT can also reasonably represent the temperature trends of air temperature.

4.4. Internal climate variability and anthropogenic climate change

This study presents the analysis results of global and regional warming status and evolution in the past decades with 0.1 and 0.05-degree spatial resolution and global land surface coverage. However, the temperature change rates revealed in those different spatial and temporal scales do not necessarily result from anthropogenic climate change only. Natural, internal climate fluctuations are also important factors in many regions on the time scale studied here. In addition, land cover and land use change, for example, have been shown to affect MODIS LST (Dutrieux et al., 2012; Nguyen et al., 2020).

Multi-decadal climate trend variability in different regions has been studied in recent literatures. McKinnon and Deser, 2018 used observational large ensemble and found that over the past 50 years, the contribution of internal variability to terrestrial climate trends is non-negligible. Bengtsson and Hodges, 2019 found that in the 20-year

trends, the variance of temperature at 2 m above the surface for Europe and the Arctic is significantly larger than for the global mean. Based on the ensemble study, it was concluded that internal processes in the climate system have played an important role in influencing decadal and multi-decadal temperature trends.

In addition, Parsons et al., 2020 identified higher variability in CMIP6 models than before, likely due to improved process representation. The Arctic was shown to have higher variability than elsewhere. However, it was also found that even the most variable models never generate unforced global temperature trends equal to the recently observed global warming trends forced by greenhouse gas emissions.

It is worth noting that in this work, we performed the empirical study based on remotely sensed data and reanalysis-driven land surface model data. Therefore, the results do not distinguish effects of internal climate variability from anthropogenic climate change.

4.5. Non-uniform warming trends among continents

Our analysis confirms that global warming has been developing differently across continents in the past decades, with temperature

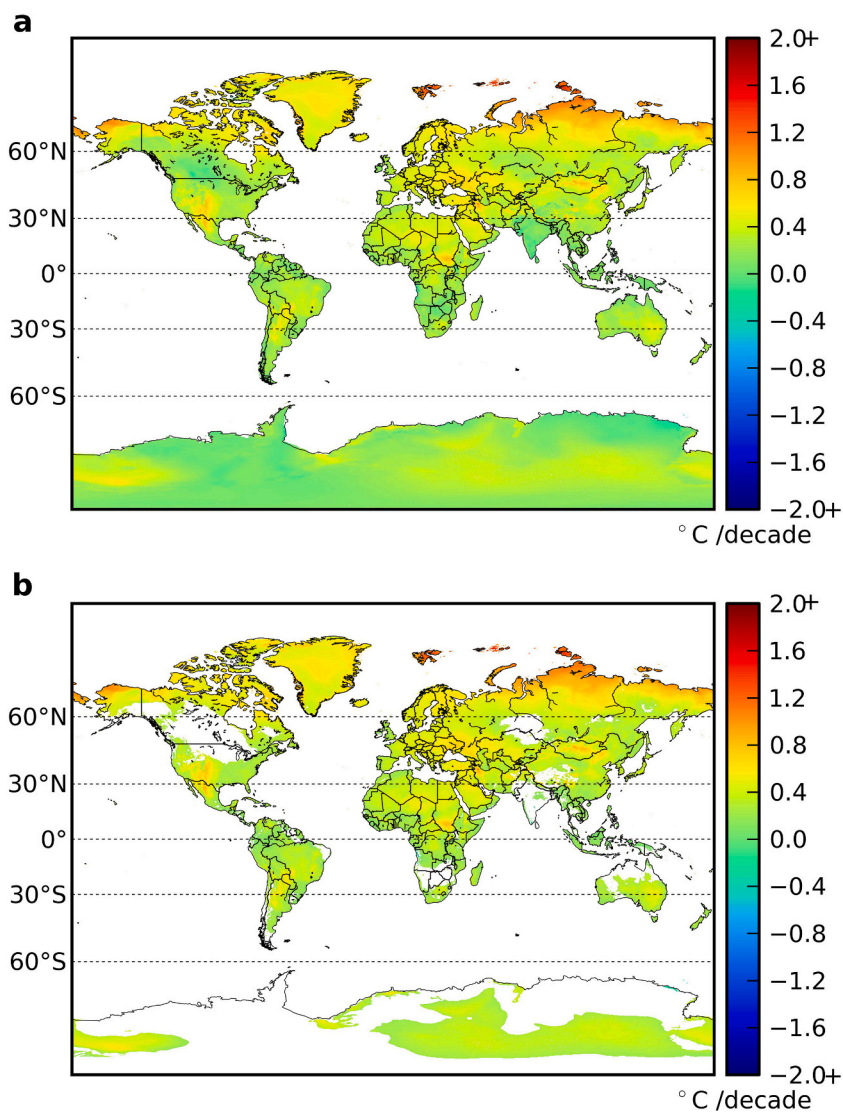


Fig. 7. Land surface temperature rate of change (°C/decade) in 1981–2020 from ERA5-Land SKT. (a) All pixels. (b) Pixels that have statistically significant rates only.

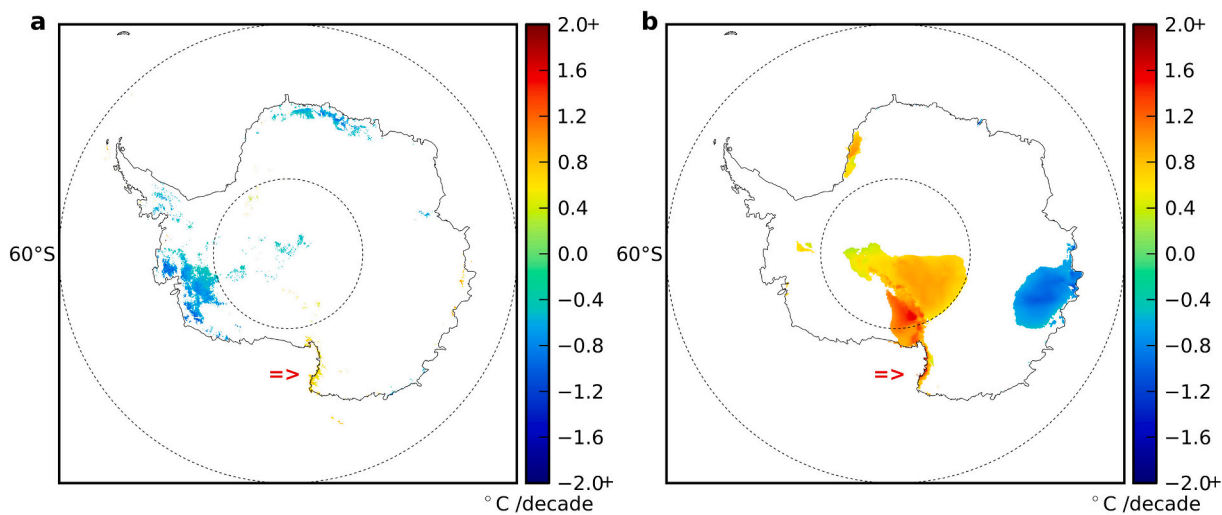


Fig. 8. Temperature rate of change of the pixels that had statistically significant trends in Antarctica in 2001–2020. (a) From MODIS LST. (b) From ERA5-Land SKT. Red arrows indicate warming areas determined by both datasets. (For interpretation of the references to colour in this figure legend, the reader is referred to the web version of this article.)

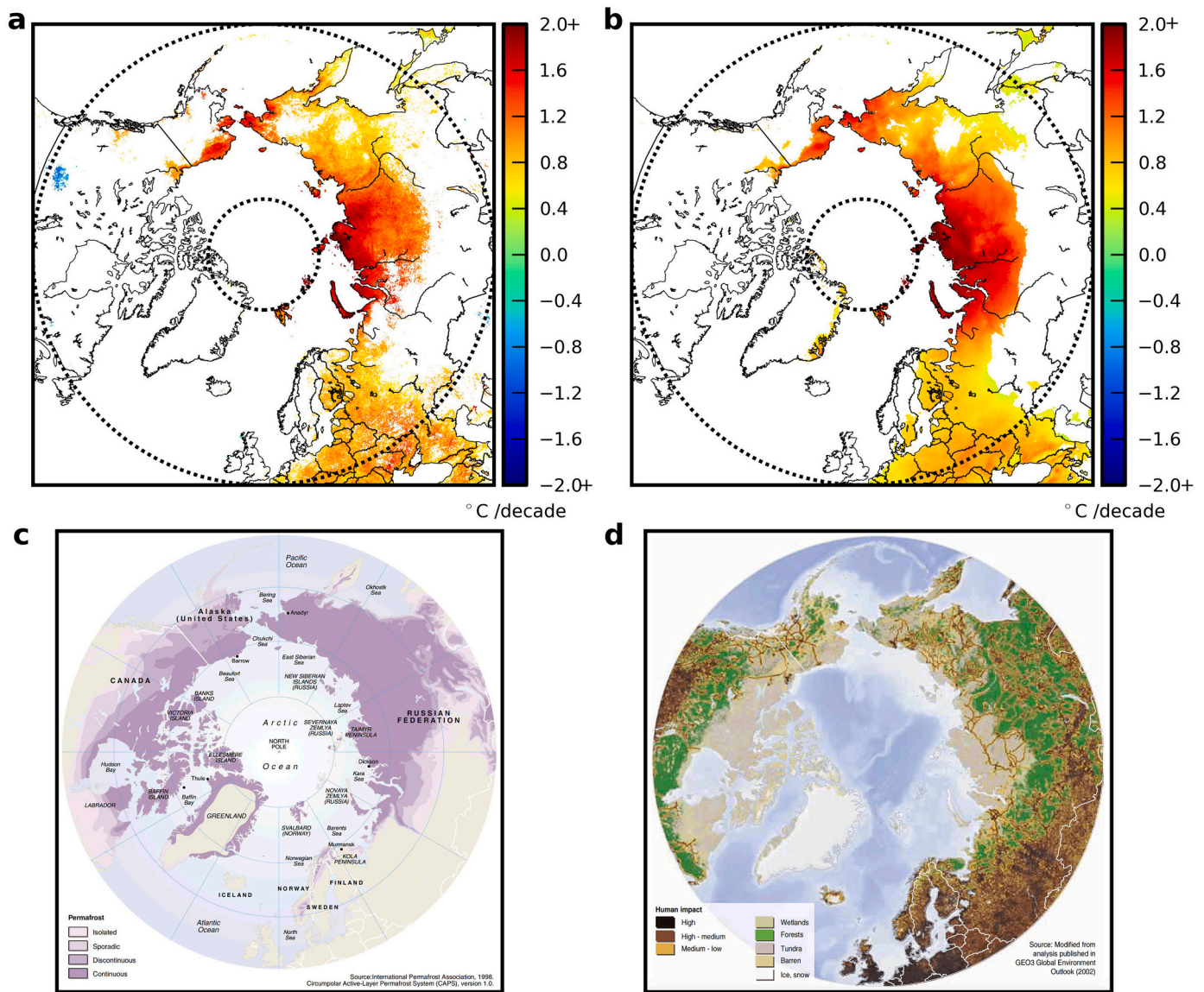


Fig. 9. Areas with significant temperature rate of change, permafrost, and land cover in the circumpolar region. (a) From MODIS LST. (b) From ERA5-Land SKT. (c) Map of circumpolar permafrost areas made by UNEP/GRID-Arendal using data from International Permafrost Association (1998). (d) Map of land cover types made by UNEP/GRID-Arendal using data from GEO3 Global Environment Outlook (2002).

change rates differing by as much as two to three times (Fig. S1). While the northern hemisphere appears to have higher warming rates than the southern, the exceptionally high temperature change rates of Europe and Russia, however, are not seen in North America being in the similar latitudinal range. This implies that regional warming trends do not depend on latitude alone, but also on other geographical conditions, as well as on decadal scale modes of internal variability.

While the full set of causes of such non-uniform warming trends among continents need more investigation, it is important that such phenomena are recognized in the public, in order that personal or regional climate experience is not misrepresented (Egan and Mullin, 2012; Weber, 2006). Under such informed understanding, GHG reduction policies and climate change adaptation measures can be more adequately established.

4.6. Arctic permafrost as the fastest warming land

In the strengthening global warming condition arising from the beginning of the 21st century, in the pixel-wise scale, the method of *p*-value-masking disclosed that the continuous permafrost in northern

Siberia and northern Alaska, in particular, is under increasing stress bearing the fastest rate of warming on earth.

In addition to feedbacks involving the Arctic sea and sea ice, the findings shown in Fig. 9 support the suggestions that the climate feedback due to tundra shrubification in the permafrost may play a prominent role in terrestrial Arctic amplification. Arctic warming has been associated with increasing shrub cover across the Arctic (Elmendorf et al., 2012), by detecting the Normalized Difference Vegetation Index, various remote sensing data have revealed 13% to 42% greening trends in Arctic tundra regions (Myers-Smith et al., 2020). In addition, shrub cover in many tundra regions are observed to increase and advance in response to climate warming (Forbes et al., 2010). Snow albedo, therefore, is lowered by taller and aerodynamically rougher shrubs, and such a mechanism creates positive feedback loops that lead to a general increase in near-surface temperatures in high-latitudes, contributing to additional regional warming (Bonfils et al., 2012; Rydsgaard et al., 2017; Zhang et al., 2013).

The increased warming in permafrost regions could imply strong feedbacks of the climate in terms of accelerating release of CO₂ (Schädel et al., 2016) and CH₄ (Koven et al., 2011) from the huge stores of organic

C (Hugelius et al., 2014), although to some extent counteracted by increase in shrub cover yielding uptake of atmospheric CO₂ (Myers-Smith et al., 2020). The uptake of CO₂, however, is overwhelmed by the carbon release to the atmosphere on average, leading to net release of carbon to the atmosphere and accelerates climate change (Schoor et al., 2020). Enhanced permafrost protection (Beer et al., 2020; Macias-Fauria et al., 2020) in the strongly warming regions, along with cooperating permafrost monitoring measures (Gao et al., 2020; Harris et al., 2009), is advisable for preventing the acceleration of thawing and carbon release.

5. Conclusions

Evaluating global and regional temperature rate of change for the 21st century is crucial in forming the scientific basis for the study of recent development of climate change. In this work, land surface temperature data from remote sensing-based MODIS and from model-based ERA5-Land were analyzed for the period 2001–2020, yielding consistent results. To explore beyond the limited 20-yr period, additional trend analyses were performed for data in the 40-yr period 1981–2020, which are available only with ERA5-Land. The results indicate that temperature trends obtained from the relatively short 20-yr period are conforming to the general trends in the 40-yr period.

Warming trends were examined in global, continental, and pixel scales with *p*-values for significance. Continents and large regions were found to be warming at substantially different rates, with the Arctic, Europe, and Russia being the fastest warming regions around the globe. In addition, with ERA5-Land data, comparison between temperature change rates of different time periods reveals that warming in the Arctic and in most of the continents is accelerating during the 40-yr period 1981–2020.

Geographically, the fastest warming land on Earth during 2001–2020 was found to coincide with the tundra biota in circumpolar regions in general. This suggests that the biota has been under rapid warming for decades, and the biological and climatic consequences are profound even if the warming can be due to internal climate variability on top of the GHG-forced climate change. Specifically, the rapid warming of the Arctic permafrost signals the acceleration of Arctic permafrost thaw and thus the deterioration of climate change in the onset of the 21st century.

CRedit authorship contribution statement

You-Ren Wang: Conceptualization, Methodology, Software, Formal analysis, Writing – original draft, Visualization. **Dag O. Hessen:** Conceptualization, Methodology, Writing – review & editing, Funding acquisition. **Bjørn H. Samset:** Methodology, Writing – review & editing, Funding acquisition. **Frode Stordal:** Methodology, Writing – review & editing, Funding acquisition.

Declaration of Competing Interest

The authors declare no competing interests.

Acknowledgements

This work was supported by the Centre for Biogeochemistry in the Anthropocene at the University of Oslo. B.H.S. acknowledges funding through the Research Council of Norway / Belmont Forum project ACROBEAR (310648). F.S. acknowledges funding from the Faculty of Mathematics and Natural Sciences at the University of Oslo through the Strategic Research Initiative project LATICE (grant no. UiO/GEO103920), and funding from the Research Council of Norway through the project EMERALD (grant no. 294948).

The authors thank the Distributed Active Archive Center (DAAC) for making and distributing the NASA MODIS/Terra Land Surface Temperature/Emissivity Monthly L3 Global 0.05 Deg CMG dataset. We also

thank the Copernicus Climate Change Service Information [2019], which is operated by the European Centre for Medium-Range Weather Forecasts (ECMWF) on behalf of the European Union, for generating and distributing the ERA5-Land skin temperature dataset. The authors are appreciative of UNEP/GRID-Arendal for creating the permafrost and land cover maps and making them publicly available.

Appendix A. Supplementary data

Supplementary data to this article can be found online at <https://doi.org/10.1016/j.rse.2022.113181>.

References

- Ahlenius, H., 2005. Human Impact on the Arctic Environment 2002, UNEP/GRID-Arendal. UNEP/GRID-Arendal.
- Akinyemi, F.O., Ikanyeng, M., Muro, J., 2019. Land cover change effects on land surface temperature trends in an African urbanizing dryland region. *City Environ. Interact.* 4, 100029.
- Allen, M., Dube, O., Solecki, W., Aragón-Durand, F., Cramer, W., Humphreys, S., Kainuma, M., Kala, J., Mahowald, N., Muloggetta, Y., 2018. Global warming of 1.5° C. An IPCC Special Report on the impacts of global warming of 1.5° C above pre-industrial levels and related global greenhouse gas emission pathways, in the context of strengthening the global response to the threat of climate change, sustainable development, and efforts to eradicate poverty. In: Sustainable Development, and Efforts to Eradicate Poverty.
- Beer, C., Zimov, N., Olofsson, J., Porada, P., Zimov, S., 2020. Protection of permafrost soils from thawing by increasing herbivore density. *Sci. Rep.* 10, 1–10.
- Benali, A., Carvalho, A., Nunes, J., Carvalhais, N., Santos, A., 2012. Estimating air surface temperature in Portugal using MODIS LST data. *Remote Sens. Environ.* 124, 108–121.
- Bengtsson, L., Hodges, K.I., 2019. Can an ensemble climate simulation be used to separate climate change signals from internal unforced variability? *Clim. Dyn.* 52, 3553–3573.
- Biskaborn, B.K., Smith, S.L., Noetzi, J., Matthes, H., Vieira, G., Streletskiy, D.A., Schoeneich, P., Romanovsky, V.E., Lewkowicz, A.G., Abramov, A., 2019. Permafrost is warming at a global scale. *Nat. Commun.* 10, 1–11.
- Bonfilis, C., Phillips, T., Lawrence, D., Cameron-Smith, P., Riley, W., Subin, Z., 2012. On the influence of shrub height and expansion on northern high latitude climate. *Environ. Res. Lett.* 7, 015503.
- Canadell, J.G., Ciais, P., Gurney, K., Le Quéré, C., Piao, S., Raupach, M.R., Sabine, C.L., 2011. An international effort to quantify regional carbon fluxes. *EOS Trans. Am. Geophys. Union* 92, 81–82.
- Chen, X., Su, Z., Ma, Y., Cleverly, J., Liddell, M., 2017. An accurate estimate of monthly mean land surface temperatures from MODIS clear-sky retrievals. *J. Hydrometeorol.* 18, 2827–2847.
- Chen, Y., Sharma, S., Zhou, X., Yang, K., Li, X., Niu, X., Hu, X., Khadka, N., 2021. Spatial performance of multiple reanalysis precipitation datasets on the southern slope of central Himalaya. *Atmos. Res.* 250, 105365.
- Ciais, P., Yao, Y., Gasser, T., Baccini, A., Wang, Y., Lauerwald, R., Peng, S., Bastos, A., Li, W., Raymond, P.A., 2021. Empirical estimates of regional carbon budgets imply reduced global soil heterotrophic respiration. *Natl. Sci. Rev.* 8, nwa145.
- Cohen, J., Screen, J.A., Furtado, J.C., Barlow, M., Whittleston, D., Coumou, D., Francis, J., Dethloff, K., Entekhabi, D., Overland, J., 2014. Recent Arctic amplification and extreme mid-latitude weather. *Nat. Geosci.* 7, 627–637.
- Coll, C., Caselles, V., Galve, J.M., Valor, E., Niclos, R., Sánchez, J.M., Rivas, R., 2005. Ground measurements for the validation of land surface temperatures derived from AATSR and MODIS data. *Remote Sens. Environ.* 97, 288–300.
- Crowhurst, D., Dadson, S., Peng, J., Washington, R., 2021. Contrasting controls on Congo Basin evaporation at the two rainfall peaks. *Clim. Dyn.* 56, 1609–1624.
- Dutrieux, L., Bartholomeus, H., Herold, M., Verbesselt, J., 2012. Relationships between declining summer sea ice, increasing temperatures and changing vegetation in the Siberian Arctic tundra from MODIS time series (2000–11). *Environ. Res. Lett.* 7, 044028.
- ECMWF, 2022. ERA5-Land monthly averaged data from 1981 to present. In: Copernicus Climate Change Service (C3S) Climate Data Store (CDS). <https://doi.org/10.24381/cds.68d2bb30?tab=overview> (accessed 16.Mar.2021).
- Egan, P.J., Mullin, M., 2012. Turning personal experience into political attitudes: the effect of local weather on Americans' perceptions about global warming. *J. Polit.* 74, 796–809.
- Eleftheriou, D., Kiachidis, K., Kalmintzis, G., Kalea, A., Bantasis, C., Koumadoraki, P., Spathara, M.E., Tsolaki, A., Tzampazidou, M.L., Gemitzi, A., 2018. Determination of annual and seasonal daytime and nighttime trends of MODIS LST over Greece-climate change implications. *Sci. Total Environ.* 616, 937–947.
- Elmendorf, S.C., Henry, G.H., Hollister, R.D., Björk, R.G., Boulanger-Lapointe, N., Cooper, E.J., Cornelissen, J.H., Day, T.A., Dorrepaal, E., Elumeeva, T.G., 2012. Plot-scale evidence of tundra vegetation change and links to recent summer warming. *Nat. Clim. Chang.* 2, 453–457.
- Forbes, B.C., Fauria, M.M., Zetterberg, P., 2010. Russian Arctic warming and 'greening' are closely tracked by tundra shrub willows. *Glob. Chang. Biol.* 16, 1542–1554.

- Forkel, M., Carvalhais, N., Verbesselt, J., Mahecha, M.D., Neigh, C.S., Reichstein, M., 2013. Trend change detection in NDVI time series: effects of inter-annual variability and methodology. *Remote Sens.* 5, 2113–2144.
- Fréville, H., Brun, E., Picard, G., Tatarinova, N., Arnaud, L., Lanconelli, C., Reijmer, C., Van den Broeke, M., 2014. Using MODIS land surface temperatures and the Crocus snow model to understand the warm bias of ERA-interim reanalyses at the surface in Antarctica. *Cryosphere* 8, 1361–1373.
- Gao, H., Nie, N., Zhang, W., Chen, H., 2020. Monitoring the spatial distribution and changes in permafrost with passive microwave remote sensing. *ISPRS J. Photogramm. Remote Sens.* 170, 142–155.
- Gulev, S.K., Thorne, P.W., Ahn, J., Dentener, F.J., Domingues, C.M., Gerland, S., Gong, D., Kaufman, D.S., Nnamchi, H.C., Quaas, J., Rivera, J.A., Sathyendranath, S., Smith, S.L., Trewin, B., Schuckmann, K.V., Vose, R.S., 2021. Chapter 2: Changing state of the climate system. In: Masson-Delmotte, V., Zhai, P., Pirani, A., Connors, S. L., Péan, C., Berger, S., Caud, N., Chen, Y., Goldfarb, L., Gomis, M.I., Huang, M., Leitzell, K., Lonnoy, E., Matthews, J.B.R., Maycock, T.K., Waterfield, T., Yelekçi, O., Yu, R., Zhou, B. (Eds.), *Climate Change 2021: The Physical Science Basis. Contribution of Working Group I to the Sixth Assessment Report of the Intergovernmental Panel on Climate Change*. Cambridge University Press. In Press.
- Hansen, J., Ruedy, R., Sato, M., Lo, K., 2010. Global surface temperature change. *Rev. Geophys.* 48.
- Harris, C., Arenson, L.U., Christiansen, H.H., Eitzelmüller, B., Frauenfelder, R., Gruber, S., Haeberli, W., Hauck, C., Hoelzle, M., Humlum, O., 2009. Permafrost and climate in Europe: monitoring and modelling thermal, geomorphological and geotechnical responses. *Earth Sci. Rev.* 92, 117–171.
- Hellmer, H.H., Kauker, F., Timmermann, R., Determann, J., Rae, J., 2012. Twenty-first-century warming of a large Antarctic ice-shelf cavity by a redirected coastal current. *Nature* 485, 225–228.
- Hugelius, G., Strauss, J., Zubrzycki, S., Harden, J.W., Schuur, E., Ping, C.-L., Schirmer, L., Grosse, G., Michaelson, G.J., Koven, C.D., 2014. Estimated stocks of circumpolar permafrost carbon with quantified uncertainty ranges and identified data gaps. *Biogeosciences* 11, 6573–6593.
- IPCC, 2021. Summary for policymakers. In: Masson-Delmotte, V., Zhai, P., Pirani, A., Connors, S.L., Péan, C., Berger, S., Caud, N., Chen, Y., Goldfarb, L., Gomis, M.I., Huang, M., Leitzell, K., Lonnoy, E., Matthews, J.B.R., Maycock, T.K., Waterfield, T., Yelekçi, O., Yu, R., Zhou, B. (Eds.), *Climate Change 2021: The Physical Science Basis. Contribution of Working Group I to the Sixth Assessment Report of the Intergovernmental Panel on Climate Change*. Cambridge University Press. In Press.
- Jones, P.D., New, M., Parker, D.E., Martin, S., Rigor, I.G., 1999. Surface air temperature and its changes over the past 150 years. *Rev. Geophys.* 37, 173–199.
- Koven, C.D., Ringeval, B., Friedlingstein, P., Ciais, P., Cadule, P., Khvorostyanov, D., Krinner, G., Tarnocai, C., 2011. Permafrost carbon-climate feedbacks accelerate global warming. *Proc. Natl. Acad. Sci.* 108, 14769–14774.
- Landrum, L., Holland, M.M., 2020. Extremes become routine in an emerging new Arctic. *Nat. Clim. Chang.* 1–8.
- Macias-Fauria, M., Jepson, P., Zimov, N., Malhi, Y., 2020. Pleistocene Arctic megafaunal ecological engineering as a natural climate solution? *Philos. Trans. R. Soc. B* 375, 20190122.
- McKinnon, K.A., Deser, C., 2018. Internal variability and regional climate trends in an observational large ensemble. *J. Clim.* 31, 6783–6802.
- Meyer, H., Katurji, M., Appelhans, T., Müller, M.U., Nauss, T., Roudier, P., Zawar-Reza, P., 2016. Mapping daily air temperature for Antarctica based on MODIS LST. *Remote Sens.* 8, 732.
- MODIS, 2022. LP DAAC - MOD11C3 v006 MODIS/Terra Land Surface Temperature/Emissivity Monthly L3 Global 0.05 Deg CMG. LP DAAC. <https://lpdaac.usgs.gov/products/mod11c3v006/> (accessed 03.Feb.2021).
- Morice, C.P., Kennedy, J.J., Rayner, N.A., Winn, J., Hogan, E., Killick, R., Dunn, R., Osborn, T., Jones, P., Simpson, I., 2020. An updated assessment of near-surface temperature change from 1850: the HadCRUT5 dataset. *J. Geophys. Res.-Atmos.* 126 (3), e2019JD032361.
- Muñoz Sabater, J., 2019. ERA5-Land Monthly Averaged Data from 1981 to Present, Copernicus Climate Change Service (C3S) Climate Data Store (CDS) (accessed 16. Mar.2021). <https://doi.org/10.24381/cds.68d2bb3>.
- Muñoz-Sabater, J., Dutra, E., Agustí-Panareda, A., Albergel, C., Arduini, G., Balsamo, G., Boussetta, S., Choulga, M., Harrigan, S., Hersbach, H., 2021. ERA5-Land: a state-of-the-art global reanalysis dataset for land applications. *Earth Syst. Sci. Data Discuss.* 1–50.
- Muro, J., Strauch, A., Heinemann, S., Steinbach, S., Thonfeld, F., Waske, B., Diekkrüger, B., 2018. Land surface temperature trends as indicator of land use changes in wetlands. *Int. J. Appl. Earth Obs. Geoinf.* 70, 62–71.
- Myers-Smith, I.H., Kerby, J.T., Phoenix, G.K., Bjerke, J.W., Epstein, H.E., Assmann, J.J., John, C., Andreu-Hayles, L., Angers-Blondin, S., Beck, P.S., 2020. Complexity revealed in the greening of the Arctic. *Nat. Clim. Chang.* 10, 106–117.
- Nguyen, L.H., Joshi, D.R., Clay, D.E., Henebry, G.M., 2020. Characterizing land cover/land use from multiple years of Landsat and MODIS time series: a novel approach using land surface phenology modeling and random forest classifier. *Remote Sens. Environ.* 238, 111017.
- Parmentier, F.-J.W., Christensen, T.R., Sørensen, L.L., Rysgaard, S., McGuire, A.D., Miller, P.A., Walker, D.A., 2013. The impact of lower sea-ice extent on Arctic greenhouse-gas exchange. *Nat. Clim. Chang.* 3, 195–202.
- Parsons, L.A., Brennan, M.K., Wills, R.C., Proistosescu, C., 2020. Magnitudes and spatial patterns of interdecadal temperature variability in CMIP6. *Geophys. Res. Lett.* 47 e2019GL086588.
- Pelosi, A., Terribile, F., D'Urso, G., Chirico, G.B., 2020. Comparison of ERA5-Land and UERRA MESCAN-SURFEX reanalysis data with spatially interpolated weather observations for the regional assessment of reference evapotranspiration. *Water* 12, 1669.
- Previdi, M., Janoski, T.P., Chiodo, G., Smith, K.L., Polvani, L.M., 2020. Arctic amplification: a rapid response to radiative forcing. *Geophys. Res. Lett.* 47 e2020GL089933.
- Rekacewicz, P., 2005. Permafrost distribution in the Arctic, UNEP/GRID-Arendal. Data from International Permafrost Association, 1998. Circumpolar Active-Layer Permafrost System (CAPS), version 1.0. In: UNEP/GRID-Arendal.
- Rydsoo, J.H., Stordal, F., Bryn, A., Tallaksen, L.M., 2017. Effects of shrub and tree cover increase on the near-surface atmosphere in northern Fennoscandia. *Biogeosciences* 14, 4209–4227.
- Samset, B., Fuglestad, J., Lund, M., 2020. Delayed emergence of a global temperature response after emission mitigation. *Nat. Commun.* 11, 1–10.
- Schädel, C., Bader, M.K.-F., Schuur, E.A., Biasi, C., Bracho, R., Capek, P., De Baets, S., Diákóvá, K., Ernakovich, J., Estop-Aragones, C., 2016. Potential carbon emissions dominated by carbon dioxide from thawed permafrost soils. *Nat. Clim. Chang.* 6, 950–953.
- Schuur, T., Bracho, R., Celis, G., Belshe, F., Ebert, C., Ledman, J., Mauritz, M., Pegoraro, E., Plaza, C., Rodenhizer, H., 2020. Tundra underlain by thawing permafrost persistently emits carbon to the atmosphere over fifteen years of measurements. *J. Geophys. Res. Biogeosci.* 126 (6), e2020JG006044.
- Serreze, M.C., Francis, J.A., 2006. The Arctic amplification debate. *Clim. Chang.* 76, 241–264.
- Shepherd, A., Wingham, D., Rignot, E., 2004. Warm ocean is eroding West Antarctic ice sheet. *Geophys. Res. Lett.* 31.
- Sheridan, S.C., Lee, C.C., Smith, E.T., 2020. A comparison between station observations and reanalysis data in the identification of extreme temperature events. *Geophys. Res. Lett.* 47 e2020GL088120.
- Stefanidis, K., Varlas, G., Vourka, A., Papadopoulos, A., Dimitriou, E., 2021. Delineating the relative contribution of climate related variables to chlorophyll-a and phytoplankton biomass in lakes using the ERA5-Land climate reanalysis data. *Water Res.* 117053.
- Tebaldi, C., Debeire, K., Eyring, V., Fischer, E., Fyfe, J., Friedlingstein, P., Knutti, R., Lowe, J., O'Neill, B., Sanderson, B., 2021. Climate model projections from the scenario model intercomparison project (ScenarioMIP) of CMIP6. *Earth Syst. Dyn.* 12, 253–293.
- van der Linden, E.C., Le Bars, D., Bintanja, R., Hazeleger, W., 2019. Oceanic heat transport into the Arctic under high and low CO₂ forcing. *Clim. Dyn.* 53, 4763–4780.
- Verbesselt, J., Hyndman, R., Newnham, G., Culvenor, D., 2010. Detecting trend and seasonal changes in satellite image time series. *Remote Sens. Environ.* 114, 106–115.
- Wan, Z., 2008. New refinements and validation of the MODIS land-surface temperature/emissivity products. *Remote Sens. Environ.* 112, 59–74.
- Wan, Z., 2013. Collection-6 MODIS Land Surface Temperature Products Users' Guide. ERI, University of California, Santa Barbara.
- Wan, Z., 2014. New refinements and validation of the collection-6 MODIS land-surface temperature/emissivity product. *Remote Sens. Environ.* 140, 36–45.
- Wan, Z., Li, Z.L., 2008. Radiance-based validation of the V5 MODIS land-surface temperature product. *Int. J. Remote Sens.* 29, 5373–5395.
- Wan, Z., Hook, S., Hulley, G., 2015. MOD11C3 MODIS/Terra Land Surface Temperature/Emissivity Monthly L3 Global 0.05 Deg CMG V006. NASA EOSDIS Land Processes DAAC (accessed 03.Feb.2021).
- Weber, E.U., 2006. Experience-based and description-based perceptions of long-term risk: why global warming does not scare us (yet). *Clim. Chang.* 77, 103–120.
- Zhang, W., Miller, P.A., Smith, B., Wania, R., Koenigk, T., Döschner, R., 2013. Tundra shrubification and tree-line advance amplify arctic climate warming: results from an individual-based dynamic vegetation model. *Environ. Res. Lett.* 8, 034023.
- Zhang, H., Zhang, F., Ye, M., Che, T., Zhang, G., 2016. Estimating daily air temperatures over the Tibetan Plateau by dynamically integrating MODIS LST data. *J. Geophys. Res.-Atmos.* 121, 11,425–411,441.